An Implicit SPH Formulation for Incompressible Linearly Elastic Solids

Andreas Peer (iD), Christoph Gissler, Stefan Band and Matthias Teschner

University of Freiburg, Germany
{peera, gisslerc, bands, teschner}@informatik.uni-freiburg.de

Abstract

We propose a novel smoothed particle hydrodynamics (SPH) formulation for deformable solids. Key aspects of our method are implicit elastic forces and an adapted SPH formulation for the deformation gradient that—in contrast to previous work—allows a rotation extraction directly from the SPH deformation gradient. The proposed implicit concept is entirely based on linear formulations. As a linear strain tensor is used, a rotation-aware computation of the deformation gradient is required. In contrast to existing work, the respective rotation estimation is entirely realized within the SPH concept using a novel formulation with incorporated kernel gradient correction for first-order consistency. The proposed implicit formulation and the adapted rotation estimation allow for significantly larger time steps and higher stiffness compared to explicit forms. Performance gain factors of up to one hundred are presented. Incompressibility of deformable solids is accounted for with an ISPH pressure solver. This further allows for a pressure-based boundary handling and a unified processing of deformables interacting with SPH fluids and rigids. Self-collisions are implicitly handled by the pressure solver.

Keywords: physically based animation, animation, fluid modelling, animation, particle systems, animation

ACM CCS: Categories and Subject Descriptors (according to ACM CCS): I.3.7 [Computer Graphics]: Three, Dimensional Graphics and Realism, Animation

1. Introduction

The smoothed particle hydrodynamics (SPH) method [Mon92] has evolved into one of the preferred choices for simulation in computer graphics. Most commonly known for the simulation of fluids [IOS*14], its Lagrangian nature makes SPH attractive for the simulation of other materials as well, with formulations proposed for unified SPH frameworks [SSP07, LD09] and in particular, for deformables [BIT09].

Whereas in the computational physics community, SPH for deformables has been an ongoing research topic, for example, [Mon12, CPDH12, Gan15, GSMH16], in the computer graphics community the focus for deformables was led to other concepts like the finite element method (FEM) [KMBG09, JK09, DGW11, SB12b, KBT17] and position-based dynamics (PBD) [BMO*14]. However, the improvements made in SPH fluid simulations in the last decade render the SPH concept an interesting alternative for the simulation of deformables in computer graphics.

One of the challenging aspects in deformable modelling is the rotation handling with SPH. If a non-linear strain measure such as the Green strain tensor is used, this is less of an issue, for example, [Gan15]. If, however, the linear infinitesimal strain tensor is used, rotations have to be estimated and used in corotational formulations, for example, [BIT09]. As we aim at an implicit formulation, we use a corotational formulation employing the linear strain tensor, which we exploit to establish a linear relation between positions and elastic forces.

In the context of the rotation extraction, one difference of our method to [BIT09] is the SPH approximation of the deformation gradient. As discussed in [BIT09], the SPH kernel gradient is not first-order consistent, which manifests in an erroneous representation of the rotation in the SPH deformation gradient. Therefore, we incorporate a correction of the kernel gradient for first-order consistency which allows to directly extract a meaningful rotation from the SPH deformation gradient. This is in contrast to [BIT09], where the rotation is extracted from an additional transformation matrix with the moving least squares (MLS) method and also in contrast
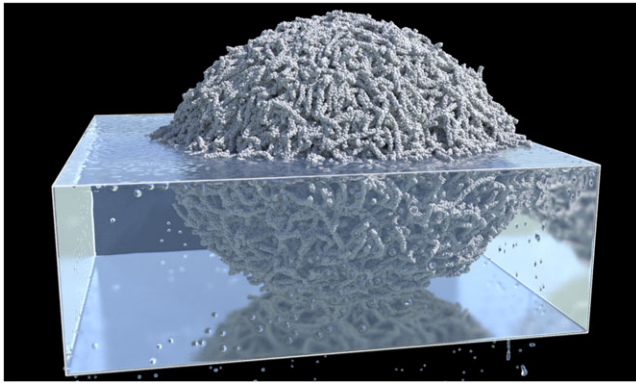
Figure 1: *Particle view of NVIDIA's highly detailed deformable hairball model floating in a fluid.*

to [SSP07] where rotations are not addressed. Thus, our proposed solution is entirely based on the SPH concept.

Another difference to previous SPH methods for deformable objects is an implicit formulation that considers forces at the next timestep in the velocity update. This generally improves the performance compared to explicit formulations and we present performance gain factors of up to one hundred. While the general concept is very popular and well established, for example, [BW98, PICT15], the particular SPH formulation for deformables is novel. Our elastic forces are linear in the positions and we end up with a linear system. We further combine the proposed solver for elastic forces with an incompressible SPH (ISPH) pressure solver [ICS*14] to gain the typical benefits such as incompressibility and pressure-based boundary handling. This enables versatile effects as illustrated in Figure 1 with complex deformable objects that interact with fluids and rigids. Self-collisions are also implicitly handled by the pressure solver and phase transitions, for example, from deformable to fluid or vice versa, can be easily simulated.

2. Related Work

Particle-based formulations have a long history for the simulation of deformable bodies in computer graphics. Among the earliest and simplest models are mass-spring systems [TPF89, MP89], which have predominately been used for 1D or 2D bodies like cloths [BW98, BFA02], but also for fully 3D models [THMG04], and have gotten new attention recently [SSF13, LBOK13]. They are fast and easy to implement, but are difficult to map to the theoretical background of elasticity in physics.

For being able to use the physical formulation of elasticity, the gradient of the deformation map or alternatively, of the displacement field needs to be evaluated. This requires a way to measure the displacement, as well as a method to compute the gradient. The former is either done by using a stored reference configuration or by incrementally updating the deformation measure. The latter is done in particle-based simulations mainly using either SPH [Mon92] or MLS [LS81]. As a physically motivated approach, SPH is a popular particle-based simulation system. Mostly known for the

simulation of fluids [IOS*14], with recent improvements in volume preservation [ICS*14, BK16, TL16], boundary handling [AIA*12, SB12a], multi-phase simulation [SP08, RLY*14] and viscosity handling [PICT15, TDF*15, BK16, PT17], its Lagrangian nature makes it appealing for the simulation of deformable objects as well, for which it has been used in computer graphics since the beginning [DG96]. It allows to compute gradients by exploiting the gradient of the smoothing kernel. However, in the standard formulation, the SPH kernel gradient evaluation is not first-order consistent, which means that it fails to capture rotational motions. As a loophole, Müller *et al.* [MKN*04] introduced MLS to the computer graphics community, which computes gradients by fitting a polynomial function. Using a linear basis, it is able to correctly capture rotational motions. However, this comes with the cost of inverting a matrix, which is tricky for colinear or coplanar particle arrangements [MKB*10]. Nevertheless, MLS has been used in a variety of works ranging from plastic deformation [JWJ*14] to fracturing [PKA*05], using either a reference configuration, or updating the deformation gradient incrementally [GBB09]. Zhou *et al.* [ZLKW13] proposed an MLS-based implicit formulation, which is similar to ours in the sense that rotation is assumed to be constant during the simulation step in order to get a linear system to solve. Their approach is, however, purely focused on elasto-plastic solids, whereas our work is not only focused on elastic solids, but also emphasizes the interplay with other material types by employing beneficial SPH formulations.

Because of its simplicity and versatility, many works prefer SPH for the simulation of deformable objects, as it fits well into a unified framework for the simulation of a wide range of materials. Keiser *et al.* [KAG*05] proposed a framework for the simulation of deformable solids and fluids. An Eulerian formulation is employed, where the displacement field is evaluated in the current configuration. An initial state, but no initial connectivity is stored. They compute pressure and viscosity forces using the SPH formalism. However, elastic forces are computed as in [MKN*04], using MLS to retrieve the gradient of the displacement field. Wicke *et al.* [WHP*06] proposed a modified MLS-based approach that does not need an initial state. Instead, they assume the particles to be aligned in a lattice, and compute a transformation for the current state that best matches the predefined lattice. Solenthaler *et al.* [SSP07] build on [KAG*05], but modify the approach in two ways. First, they use a Lagrangian formulation where the displacement field is evaluated in a stored reference configuration. Second, they use SPH for all computations. However, as the default SPH kernel gradient computation is not first-order consistent, they fail to correctly capture rigid-body rotations of their deformable objects. Becker *et al.* [BIT09] noted this and switched back to an MLS–SPH combined approach, but in contrast to [KAG*05], they use MLS just for extracting the rotational part of the deformation gradient, and further use a corotated [MDM*02] SPH formulation that incorporates the obtained rotation information. In contrast to all those works, we solely rely on SPH for capturing rotations. Furthermore, instead of using explicit force computations, we propose an implicit formulation that allows for significantly larger timesteps.

Apart from models with physical elasticity, SPH has also been combined with simpler formulations like mass-spring systems for the interaction with thin shells [LD08] or for viscoelastic flow

[CBP05]. As a simple model for elasticity, Dagenais *et al.* [DGP12] proposed to use shape matching [MHTG05] to blend fluid and solid motion in order to mimic deformable objects.

Since computing the gradient is a non-trivial task on a randomly arranged particle set, but comparatively easy on a regular grid, the material point method (MPM) uses an underlying grid for the force computation and has been used for phase changes [SSJ*14] and dimension-reduced deformables [JGT17]. In each simulation step, the required quantities are transferred from the particles to the grid, where the forces are computed, and the resulting changes are transferred back to the Lagrangian particles. As we employ a kernel correction, we are able to reliably compute all relevant quantities on a randomly arranged particle set, and we do not need the additional grid.

Another alternative for gradient computations with a particular focus on discontinuities is proposed within the peridynamics concept [Sil00]. This concept has also recently been used for the simulation of elastoplastic materials [HWW17]. Depending on the application, there is a close relation between SPH and peridynamics. If peridynamics is, for example, applied to classical material models based on the deformation gradient, Ganzenmüller *et al.* [GHM15] show that the resulting forces exactly match a respective SPH discretization.

Beside particle-based formulations, a great variety of methods have been used to simulate deformable objects in computer graphics, with FEM [SB12b] being one of the most common choices. We refer the reader to [NMK*06] for a slightly outdated, but still excellent overview of the different methods. Recently, PBD [MHHR07, BMO*14] and its generalization, the projective dynamics framework [BML*14] got attention for the simulation of a great variety of materials, from fluids [MM13, WKB16] to solids [MC11] and a wide range of deformable materials, for example, [BKCW14, CMM16, MMC16, LBK16, NOB16, TDFN16]. Its constrained-based nature makes it attractive for the unified simulation of objects with different material characteristics as well [MMCK14].

3. Method

3.1. Background and notation

Using a continuum-mechanics framework, elastic materials are characterized by an initial or reference configuration $\mathbf{x}^0$ and the current configuration $\mathbf{x}$. In this work, we will use the superscript $*^0$ to denote quantities in the initial configuration. Elastic forces act to bring an object from its current shape back to its initial shape. The deformation function ϕ maps the initial configuration to the current configuration $\mathbf{x} = \phi(\mathbf{x}^0)$. The deformation gradient $\mathbf{F} = \nabla^0 \phi = \frac{\partial \phi}{\partial \mathbf{x}^0} = \frac{\partial \mathbf{x}}{\partial \mathbf{x}^0}$ states how the deformation changes spatially. The displacement $\mathbf{u} = \mathbf{x} - \mathbf{x}^0$ is an alternative measure. Its gradient is given by $\nabla^0 \mathbf{u} = \mathbf{F} - \mathbf{I}$. For Cauchy elastic materials, the stress tensor from which the elastic forces are computed solely depends on $\mathbf{F}$.

We generally employ the SPH concept for the spatial discretization of all relevant equations. In SPH, a continuum volume is approximately represented by samples or particles. For the computation of a quantity A_i at position $\mathbf{x}_i$, a weighted average over neighbouring particles at positions $\mathbf{x}_j$ is employed: $A_i = \sum_j V_j A_j W_{ij}$. The value V_j represents the volume of the particle at $\mathbf{x}_j$ and $W_{ij} = W(\mathbf{x}_i - \mathbf{x}_j)$ is the smoothing kernel. Similarly, the gradient can be computed, for example, with $\nabla A_i = \sum_j V_j A_j \nabla W_{ij}$ with $\nabla W_{ij} = \nabla W(\mathbf{x}_i - \mathbf{x}_j)$ being the gradient of the smoothing kernel.

3.2. Lagrangian SPH

The distinction between initial and current configuration rises the question on which neighbourhood to use for the SPH interpolation. For fluids, that typically show no elastic behaviour, the well-known Eulerian SPH is used, where the neighbourhood is evaluated using the current particle positions. Here, the term *Eulerian* denotes the characteristic that when looking at a single particle, other particles enter and leave its influence sphere frequently. For deformables, however, it has been shown that the Eulerian formulation leads to the tensile instability problem and that a Lagrangian formulation removes it [BGLX00, BK01]. In *Lagrangian SPH*, the initial positions are used for finding the neighbourhood and therefore, the set of particles interacting with each other is kept fixed. In the following, all SPH interpolations regarding the elastic force use the initial neighbourhood. To reflect that in the formulas, we use the notation $\sum_j^0$ to denote a sum over the particles in the initial neighbourhood.

3.3. Overview

Algorithm 1 summarizes the general steps of the deformable update procedure. The main novelties compared to previous works lie in the computation of the deformation gradient as well as in the implicit application of the resulting force, which will be explicated in Section 3.4. In this section, each step of the update procedure will be introduced in detail.

Algorithm 1 Deformable update

Extract rotation
    compute deformation gradient $\mathbf{F}$
    extract rotational component $\mathbf{R}$ from $\mathbf{F}$

Compute elastic force using the extracted rotation
    compute corotated deformation gradient $\overset{\star}{\mathbf{F}}$ using $\mathbf{R}$
    compute strain tensor ε from $\overset{\star}{\mathbf{F}}$
    compute stress tensor $\mathbf{P}$ from ε
    compute elastic force $\mathbf{f}$ from $\mathbf{P}$

3.3.1. *Deformation gradient*

The proper computation of the deformation gradient $\mathbf{F} = \frac{\partial \mathbf{x}}{\partial \mathbf{x}^0}$ is the basis for implementing a deformable model. However, a trivial implementation in SPH as $\mathbf{F}_i = \sum_j^0 V_j^0 \mathbf{x}_j \otimes \nabla W(\mathbf{x}_{ij}^0)$, with $\mathbf{x}_{ji} = \mathbf{x}_j - \mathbf{x}_i$ the distance vector, fails to capture rotational motion. As pointed out by Bonet and Lok [BL99], this is due to the fact the common SPH kernel gradient interpolation is not first-order consistent. Therefore, rotations are misinterpreted as deformations. As a consequence, the employed elastic forces are not rotationally invariant. Instead, forces are induced that rotate the object back to its initial orientation.

The deformation gradient acts as a transformation matrix that transforms an infinitesimal line element $d\mathbf{x}^0$ from an initial position to the current position, as $\frac{\partial \mathbf{x}}{\partial \mathbf{x}^0} d\mathbf{x}^0 = d\mathbf{x}$. This opens up other possibilities for computing the deformation gradient. Becker *et al.* [BIT09] employed shape matching—an MLS approach—to compute the deformation gradient for extracting rotation. In our work, we adopt the corotational concept of [BIT09], but propose an alternative SPH approximation for the deformation gradient that allows to extract the rotation directly from the SPH deformation gradient. MLS is avoided and the entire procedure relies on SPH only.

3.3.2. *Rotation-aware kernel gradient*

In order to correctly capture rotational motion with the SPH kernel gradient, it has to be ensured that its computation is first-order consistent. As shown by Bonet and Lok [BL99], for the kernel gradient to be first-order consistent, the condition $\sum_j^0 V_j^0 \mathbf{x}_{ij} \otimes \nabla W(\mathbf{x}_{ij}^0) = \mathbf{I}$ has to be satisfied. For this sake, they propose a correction matrix

$$\mathbf{L}_i = \left(\sum_j^0 V_j^0 \nabla W \left(\mathbf{x}_{ij}^0 \right) \otimes \mathbf{x}_{ji}^0 \right)^{-1} \tag{1}$$

and compute the corrected kernel gradient as

$$\nabla \tilde{W}_i \left(\mathbf{x}_{ij}^0 \right) = \mathbf{L}_i \nabla W \left(\mathbf{x}_{ij}^0 \right). \tag{2}$$

This ensures first-order consistency, as $\sum_j^0 V_j^0 \mathbf{x}_{ji}^0 \otimes \nabla \tilde{W}_i(\mathbf{x}_{ij}^0) = \mathbf{I}$ is satisfied by construction. In Lagrangian SPH, the correction matrix is computed in the initial configuration and therefore, it has to be computed only once at the beginning of the simulation. For coplanar or collinear particle configurations, the matrix in Equation (1) is singular. In such cases, we compute its MoorePenrose pseudoinverse, instead.

3.3.3. *Rotation extraction*

As the corrected kernel gradient is able to capture rotations, it is straightforward to use a non-linear strain measure such as the Green strain tensor, given as $\mathbf{E} = \frac{1}{2}(\mathbf{F}^T \mathbf{F} - \mathbf{I})$. However, with the Green strain tensor, the elastic force is non-linear in the position. For an implicit formulation, this is unfavourable, as it requires to solve a non-linear system. In such a situation, one would prefer to use the infinitesimal strain tensor, given as $\boldsymbol{\varepsilon} = \frac{1}{2}(\mathbf{F} + \mathbf{F}^T) - \mathbf{I}$, where the force linearly depends on position, and the implicit formulation results in a more efficient linear system. Therefore, inspired by the corotational formulation of Becker *et al.* [BIT09], we extract rotation—which is responsible for non-linearity—beforehand. Doing so, we are able to use a strain measure linear in position. In contrast to Becker *et al.*, using the corrected kernel gradient, rotation can be extracted directly from the deformation gradient computed as

$$\mathbf{F}_i = \sum_j^0 V_j^0 \mathbf{x}_{ji} \otimes \nabla \tilde{W}_i \left(\mathbf{x}_{ij}^0 \right). \tag{3}$$

To extract the per-particle rotation $\mathbf{R}_i$ from $\mathbf{F}_i$, we use the method of Müller *et al.* [MBCM16] which is fast and stable.

3.3.4. *Corotated deformation gradient*

Similar to Becker *et al.* [BIT09], we use the extracted rotation for computing a corotated deformation gradient that only contains shear and expansion parts. Because of objectivity of Cauchy elastic materials, the computed stress tensor, and therefore the elastic force, is invariant to rotation. This allows us to compute all quantities in an arbitrary rotational frame, as long as we make sure the resulting forces are rotated back to the actual frame. Using the per-particle rotation extracted above, Becker *et al.* propose to compute the corotated deformation gradient by means of the displacement field as $\mathbf{F} = \mathbf{I} + \nabla^0 \mathbf{u} = \mathbf{I} + \nabla^0 (\mathbf{x} - \mathbf{x}^0)$ and by further rotating the current positions back to the initial positions which translates to SPH as $\mathbf{F}_i = \mathbf{I} + \sum_j^0 V_j^0 (\mathbf{R}_i^{-1} \mathbf{x}_{ji} - \mathbf{x}_{ji}^0) \otimes \nabla W(\mathbf{x}_{ij}^0)$. We modify this computation in the following way. Instead of rotating the current configuration back to the initial configuration, we rotate the initial configuration to the current configuration. Doing so, we have to rotate all initial quantities, which means that the corrected kernel has to be evaluated in the current frame as well. For that, we introduce the rotated kernel gradient as

$$\nabla \overset{\star}{W}_i \left(\mathbf{x}_{ij}^0 \right) = \mathbf{R}_i \mathbf{L}_i \nabla W \left(\mathbf{x}_{ij}^0 \right) \tag{4}$$

which rotates the corrected kernel gradient to the frame of the current configuration. With these modifications, the deformation gradient is finally computed as

$$\overset{\star}{\mathbf{F}}_i = \mathbf{I} + \sum_j^0 V_j^0 \left(\mathbf{x}_{ji} - \mathbf{R}_i \mathbf{x}_{ji}^0 \right) \otimes \nabla \overset{\star}{W}_i \left(\mathbf{x}_{ij}^0 \right). \tag{5}$$

Note that in this computation of the deformation gradient, only displacements in the initial configuration are pre-factored by the rotation matrix. This will turn advantageous when introducing the implicit formulation, as those costly matrix–vector multiplications have to be performed only once during the set-up of the system to solve, reducing the cost of each solver iteration.

3.3.5. *Linear elasticity*

As a constitutive model, we use the linear elasticity material model. Its linearity in position results in a linear system for our implicit formulation, which greatly reduces the computational effort for solving the system.

Strain: The strain tensor used in the linear elasticity model is the infinitesimal strain tensor

$$\boldsymbol{\varepsilon}_i = \frac{1}{2} \left(\overset{\star}{\mathbf{F}}_i + \overset{\star}{\mathbf{F}}_i^T \right) - \mathbf{I}. \tag{6}$$

In contrast to the Green strain tensor $\mathbf{E} = \frac{1}{2}(\mathbf{F}^T \mathbf{F} - \mathbf{I})$, position does not appear quadratically, but only linear.

Stress: In the linear elasticity model, stress depends linearly on strain. The first Piola–Kirchhoff stress tensor $\mathbf{P}$ is given as

$$\mathbf{P}_i = 2\mu \boldsymbol{\varepsilon}_i + \lambda \text{tr}(\boldsymbol{\varepsilon}_i)\mathbf{I} \tag{7}$$

with the Lamé parameters λ and μ. Alternatively, the stress tensor can be decomposed into a volumetric and a deviatoric part,

$$\mathbf{P}_i = 2G\left(\varepsilon_i - \frac{1}{3}\mathrm{tr}(\varepsilon_i)\mathbf{I}\right) + K\,\mathrm{tr}(\varepsilon_i)\mathbf{I}$$

$$= 2G\varepsilon_i + \left(K - \frac{2}{3}G\right)\mathrm{tr}(\varepsilon_i)\mathbf{I} \qquad (8)$$

with shear modulus $G = \mu$ and bulk modulus $K = \lambda + \frac{2\mu}{3}$. We parameterize the simulations in our experiments with those moduli.

3.3.6. *Elastic force*

We compute the elastic force from the divergence of the stress tensor, which in the simplest case can be computed as $\mathbf{f}_i = \sum_j^0 V_i V_j^0 (\mathbf{P}_i + \mathbf{P}_j)\nabla W(\mathbf{x}_{ij}^0)$. Note that in contrast to [BIT09], we do not rotate the force, as we compute the deformation gradient in the current frame already. However, as the rotated and corrected kernel depends on the particle of evaluation, to get a symmetric force, each stress tensor has to be multiplied by the corresponding kernel gradient separately [Gan15], resulting in

$$\mathbf{f}_i = \sum_j^0 V_i^0 V_j^0 \left(\mathbf{P}_i \overset{\star}{\nabla} W_i \left(\mathbf{x}_{ij}^0\right) - \mathbf{P}_j \overset{\star}{\nabla} W_j \left(\mathbf{x}_{ji}^0\right)\right). \qquad (9)$$

3.4. Implicit formulation

The previous section has explained all equations that are used in our computation of the elastic force. Depending on the choice of arguments, it translates to either an explicit or an implicit formulation. When approximately assuming the extracted rotation to remain constant during the simulation step, the elastic force in Equation (9) can be regarded as a function $\mathbf{f}(\mathbf{d}, \mathbf{d}^0)$ that linearly depends on two position vectors $\mathbf{d}$ and $\mathbf{d}^0$. The function is given as

$$\begin{aligned}\mathbf{f}_i(\mathbf{d}, \mathbf{d}^0) = \sum_j^0 V_i^0 V_j^0 \Big(&\mathbf{P}_i(\mathbf{d}, \mathbf{d}^0)\overset{\star}{\nabla} W_i \left(\mathbf{x}_{ij}^0\right)\\ &-\mathbf{P}_j(\mathbf{d}, \mathbf{d}^0)\overset{\star}{\nabla} W_j \left(\mathbf{x}_{ji}^0\right)\Big)\end{aligned} \qquad (10)$$

with stress, strain and the deformation gradient expressed similarly as

$$\mathbf{P}_i(\mathbf{d}, \mathbf{d}^0) = 2G\varepsilon_i(\mathbf{d}, \mathbf{d}^0) + \left(K - \frac{2}{3}G\right)\mathrm{tr}\big(\varepsilon_i(\mathbf{d}, \mathbf{d}^0)\big)\mathbf{I}, \quad (11)$$

$$\varepsilon_i(\mathbf{d}, \mathbf{d}^0) = \frac{1}{2}\left(\overset{\star}{\mathbf{F}}_i(\mathbf{d}, \mathbf{d}^0) + \overset{\star}{\mathbf{F}}_i(\mathbf{d}, \mathbf{d}^0)^T\right) - \mathbf{I}, \qquad (12)$$

$$\overset{\star}{\mathbf{F}}_i(\mathbf{d}, \mathbf{d}^0) = \mathbf{I} + \sum_j^0 V_j^0 \left(\mathbf{d}_{ji} - \mathbf{R}_i\mathbf{d}_{ji}^0\right) \otimes \overset{\star}{\nabla} W_i \left(\mathbf{x}_{ij}^0\right). \qquad (13)$$

For the explicit formulation, the two parameters are given by the position at the current timestep and the initial position, that is, $\mathbf{d} = \mathbf{x}^t$

and $\mathbf{d}^0 = \mathbf{x}^0$, respectively. The explicit velocity update can then be written as

$$\mathbf{v}_{exp}^{t+\Delta t} = \mathbf{v}^t + \Delta t\frac{\mathbf{f}(\mathbf{x}^t, \mathbf{x}^0)}{m} \qquad (14)$$

with m denoting the particle mass. For an implicit formulation, the position at the next timestep is used instead, such that $\mathbf{d} = \mathbf{x}^{t+\Delta t}$, and the velocity update changes to

$$\mathbf{v}_{imp}^{t+\Delta t} = \mathbf{v}^t + \Delta t\frac{\mathbf{f}(\mathbf{x}^{t+\Delta t}, \mathbf{x}^0)}{m}. \qquad (15)$$

Using a backward difference for the position at the next timestep, $\mathbf{x}^{t+\Delta t} = \mathbf{x}^t + \Delta t\mathbf{v}^{t+\Delta t}$, the implicit velocity update is given as

$$\mathbf{v}^{t+\Delta t} = \mathbf{v}^t + \Delta t\frac{\mathbf{f}(\mathbf{x}^t + \Delta t\mathbf{v}^{t+\Delta t}, \mathbf{x}^0)}{m}, \qquad (16)$$

where the velocity subscript has been omitted for readability. As we assume the rotation to remain constant during the update, the elastic force linearly depends on the position, and the computation of $\mathbf{f}$ can be split into $\mathbf{f}(\mathbf{x}^t + \Delta t\mathbf{v}^{t+\Delta t}, \mathbf{x}^0) = \mathbf{f}(\mathbf{x}^t, \mathbf{x}^0) + \mathbf{f}(\Delta t\mathbf{v}^{t+\Delta t}, \mathbf{0})$ to get

$$\mathbf{v}^{t+\Delta t} - \Delta t\frac{\mathbf{f}(\Delta t\mathbf{v}^{t+\Delta t}, \mathbf{0})}{m} = \mathbf{v}^t + \Delta t\frac{\mathbf{f}(\mathbf{x}^t, \mathbf{x}^0)}{m}, \qquad (17)$$

where $\mathbf{0}$ denotes the zero vector. This forms a linear system $\mathbf{A}\mathbf{v}^{t+\Delta t} = \mathbf{b}$ for the unknown velocities at the next timestep.

Discussion: In our implicit formulation, we use the simplifying assumption that the rotations remain constant during each simulation step. This allows to extract the rotations beforehand and therefore, to derive corotated forces that are linear in positions. This largely reduces the computational effort for solving the resulting system. A similar assumption is taken in [ZLKW13]. With fixed rotations, the simulation outcome will slightly differ compared to a non-linearized formulation, as potential rotation changes are not considered. In practice, however these changes are rather small and the simulations look plausible.

The system in Equation (17) shares some similarities with the system for implicit viscous forces in [TDF*15], as both viscous and elastic forces are computed from the divergence of a stress tensor. In fact, the system in [TDF*15] can be regarded a special case of our system with no rotation handling and kernel correction employed. In contrast to [TDF*15], we do not pursue to extract the coefficients of the system matrix, but we propose a more efficient matrix-free implementation, instead.

4. Implementation

4.1. Initial configuration

In the course of the deformables update, no initial positions, but initial distance vectors are processed. Therefore, following [SSP07] and [BIT09], we do not store the absolute initial position $\mathbf{x}_i$ of a particle, but the distance vectors to its neighbours $\mathbf{x}_{ji}$, instead.

Whenever new particles are inserted, a neighbourhood search is performed and the initial distance vectors for all particle–neighbour pairs are stored. Furthermore, the kernel correction matrix is precomputed using Equation (1) and stored for each particle.

4.2. Solving the system

For our deformable formulation, the linear system in Equation (17) needs to be solved. We propose a matrix-free implementation to efficiently achieve this using the conjugate gradient method. This is accomplished in three steps. First, we precompute and store the rotated kernel gradient for each particle–neighbour pair by evaluating Equation (4). Then, we compute the right-hand side of Equation (17). Finally, we solve the system iteratively.

Both the computation of the left-hand side and the right-hand side require the evaluation of the elastic force function in Equation (10). It can be evaluated efficiently by iterating twice over all particles and their neighbours, as outlined in Algorithm 2. In the first iteration, we loop once over all neighbours to compute $\overset{\star}{\mathbf{F}}$ using Equation (13), and we hereupon compute $\boldsymbol{\varepsilon}$ and $\mathbf{P}$ using Equation (12) and Equation (11), respectively. Finally, we store $\mathbf{P}$. As it is symmetric, only six independent components need to be stored. Then, in the second iteration, we loop once again over all neighbours to compute the divergence of $\mathbf{P}$ using Equation (10).

Algorithm 2 Computation of $\mathbf{f}(\mathbf{d}, \mathbf{d}^0)$

---

for all particle i **do**

$\quad \overset{\star}{\mathbf{F}}_{temp} = \mathbf{I} + \sum_j^0 V_j^0 \left(\mathbf{d}_{ji} - \mathbf{R}_i \mathbf{d}_{ji}^0 \right) \otimes \nabla \overset{\star}{W}_i \left(\mathbf{x}_{ij}^0 \right)$

$\quad \varepsilon_{temp} = \frac{1}{2} \left(\overset{\star}{\mathbf{F}}_{temp} + (\overset{\star}{\mathbf{F}}_{temp})^T \right) - \mathbf{I}$

$\quad \mathbf{P}_i = 2G\varepsilon_{temp} + \left(K - \frac{2}{3}G \right) \mathrm{tr}(\varepsilon_{temp}) \mathbf{I}$

for all particle i **do**

$\quad \mathbf{f}_i = \sum_j^0 V_i^0 V_j^0 \left(\mathbf{P}_i \nabla \overset{\star}{W}_i \left(\mathbf{x}_{ij}^0 \right) - \mathbf{P}_j \nabla \overset{\star}{W}_j \left(\mathbf{x}_{ji}^0 \right) \right)$

Right-hand side: The right-hand side of Equation (17) just computes the velocity update due to an explicit elastic force as in Equation (14), which can be computed by iterating twice over all particles and neighbours as described above. Moreover, when using the corrected kernel gradient, the computation of the corotated deformation gradient as in Equation (13) simplifies to

$$\overset{\star}{\mathbf{F}}_i(\mathbf{x}, \mathbf{x}^0) = \sum_j^0 V_j^0 \mathbf{x}_{ji} \otimes \nabla \overset{\star}{W}_i \left(\mathbf{x}_{ij}^0 \right), \qquad (18)$$

as $\sum_j^0 V_j^0 \mathbf{R}_i \mathbf{x}_{ji}^0 \otimes \nabla \overset{\star}{W}_i(\mathbf{x}_{ij}^0) = \mathbf{I}$. Strain, stress and force are then computed as usual using the respective Equations (10) to (12).

Solver iteration: In each iteration, the matrix–vector product $\mathbf{Ap}$, with $\mathbf{p}$ the basis vector in case of the conjugate gradient method, has to be computed. We do not build the matrix $\mathbf{A}$ explicitly, but rather compute the product, which is given by the left-hand side of Equation (17) for each particle as

$$(\mathbf{Ap})_i = \mathbf{p}_i - \frac{\Delta t}{m} \mathbf{f}_i(\Delta t \mathbf{p}, \mathbf{0}). \qquad (19)$$

The complexity lies in computing the elastic force $\mathbf{f}$. However, as shown above, this can be efficiently done by iterating twice over all particles and neighbours. The first iteration in the procedure described above, which consists in the computation of the deformation gradient and the strain and stress tensors, can further be slightly optimized. We note that when computing the corotated deformation gradient using Equation (13) as

$$\overset{\star}{\mathbf{F}}_i(\Delta t \mathbf{p}, \mathbf{0}) = \mathbf{I} + \Delta t \sum_j^0 V_j^0 \mathbf{p}_{ji} \otimes \nabla \overset{\star}{W}_i \left(\mathbf{x}_{ij}^0 \right), \qquad (20)$$

and strain using Equation (12) as

$$\boldsymbol{\varepsilon}_i(\Delta t \mathbf{p}, \mathbf{0}) = \frac{1}{2} \left(\overset{\star}{\mathbf{F}}_i(\Delta t \mathbf{p}, \mathbf{0}) + \left(\overset{\star}{\mathbf{F}}_i(\Delta t \mathbf{p}, \mathbf{0}) \right)^T \right) - \mathbf{I}, \qquad (21)$$

the addition of $\mathbf{I}$ in the deformation gradient is cancelled by its subtraction in the strain tensor. Therefore, following most computer graphics papers, in lieu of the deformation gradient, we compute the gradient of the displacement field as $\nabla^0 \mathbf{u} = \mathbf{F} - \mathbf{I}$, resulting in

$$\nabla^{\overset{\star}{0}} \mathbf{u}_i(\Delta t \mathbf{p}, \mathbf{0}) = \Delta t \sum_j^0 V_j^0 \mathbf{p}_{ji} \otimes \nabla \overset{\star}{W}_i \left(\mathbf{x}_{ij}^0 \right). \qquad (22)$$

Strain is then computed as

$$\boldsymbol{\varepsilon}_i(\Delta t \mathbf{p}, \mathbf{0}) = \frac{1}{2} \left(\nabla^{\overset{\star}{0}} \mathbf{u}_i(\Delta t \mathbf{p}, \mathbf{0}) + \left(\nabla^{\overset{\star}{0}} \mathbf{u}_i(\Delta t \mathbf{p}, \mathbf{0}) \right)^T \right), \qquad (23)$$

and we can continue with the calculation of stress as usual.

4.3. Conjugate gradient method

In our implementation, we use the conjugate gradient method for solving the linear system, which requires a symmetric system matrix in order to converge. From Equations (10), (13) and (17) it follows that this requires the same initial volume and the same mass for all particles. Therefore, in addition to assigning all particles the same mass $m_0 = h^3 \rho_0$ with h denoting the particle spacing and ρ_0 the rest density, we initially distribute the particles homogeneously to the given volume. Then, all particles have the same mass m_0 and roughly the same volume $V_0^0 = \frac{m_0}{\rho_0}$. With these assumptions, the system matrix is symmetric. As stopping criterion, we use the average absolute per-particle error of the system. In our experiments, this error is set to 1×10^{-3}. Furthermore, to improve convergence, we perform a 'warm start' by initializing the solver with the temporary intermediate velocity $\mathbf{v}^t + \Delta t_c \mathbf{a}^*$, as introduced in the next section.

4.4. Embedding in the fluid solver

Our elastic solver is integrated into an IISPH framework as outlined in Algorithm 3. The IISPH pressure solver accounts for collision handling and incompressibility. As correct collision handling is crucial for the simulation, the pressure solver is executed as the last step

of the fluid update. However, the accelerations induced by elastic forces may introduce high velocities that violate the CFL condition and thus undermine collision handling. Therefore, our proposed update procedure is as follows. First, we estimate a candidate timestep Δt_c from the current velocities. We compute intermediate accelerations $\mathbf{a}^*$ induced by gravity, viscosity and friction. We use the candidate timestep to integrate to a temporary intermediate velocity $\mathbf{v}^t + \Delta t_c \mathbf{a}^*$, for which the elastic system in Equation (17) is solved. The system to solve is

$$\mathbf{v}_{elast} - \Delta t_c \frac{\mathbf{f}(\Delta t_c \mathbf{v}_{elast}, \mathbf{0})}{m} = \mathbf{v}^t + \Delta t_c \left(\mathbf{a}^* + \frac{\mathbf{f}(\mathbf{x}^t, \mathbf{x}^0)}{m} \right), \quad (24)$$

where compared to Equation (17) the current velocity has been replaced by the intermediate velocity, such that the right-hand side incorporates the velocity change induced by explicit forces. With the solution velocities $\mathbf{v}_{elast}$, the timestep is re-estimated in order to ensure that the CFL condition is still satisfied. Pressure projection as well as velocity and position integration is then done using the re-estimated timestep.

Algorithm 3 Deformable SPH fluid solver

estimate candidate timestep Δt_c from $\mathbf{v}^t$
compute gravity, viscosity and friction to get acceleration $\mathbf{a}^*$
extract rotations using $\mathbf{x}^t$
solve $\mathbf{v}_{elast} - \Delta t_c \frac{\mathbf{f}(\Delta t_c \mathbf{v}_{elast}, \mathbf{0})}{m} = \mathbf{v}^t + \Delta t_c \left(\mathbf{a}^* + \frac{\mathbf{f}(\mathbf{x}^t, \mathbf{x}^0)}{m} \right)$
update acceleration: $\mathbf{a}^{**} \leftarrow \frac{\mathbf{v}_{elast} - \mathbf{v}^t}{\Delta t_c}$
estimate timestep Δt from $\mathbf{v}_{elast}$
compute press. and press. force using $\mathbf{v}^t$, $\mathbf{a}^{**}$ and Δt to get $\mathbf{a}^{***}$
update velocity: $\mathbf{v}^{t+\Delta t} \leftarrow \mathbf{v}^t + \Delta t \mathbf{a}^{***}$
update position: $\mathbf{x}^{t+\Delta t} \leftarrow \mathbf{x}^t + \Delta t \mathbf{v}^{t+\Delta t}$

---

5. Results

This section illustrates the properties of our proposed SPH-based deformables solver. Our solver is integrated into an IISPH framework [ICS*14]. As kernel, the quintic formulation of Wendland (Wendland C^2) is used [Wen95] with a support radius of twice the particle spacing. From a theoretical perspective, this kernel avoids the pairing instability [DA12]. In practice, however, we did not experience differences to the commonly used Cubic spline kernel which works as well in our setting. Boundary handling and two-way coupling is done using particles [AIA*12]. For multi-phase simulations, the number density approach is employed [SP08] with an additional surface tension force based on [AAT13] for the water phase. We further use a drag force for all phases [GBP*17] and employ XSPH viscosity [Mon89, SB12a] in the material space. A viscosity force as in [MFZ97] is used to model friction at the rigid interface. Particles for deformable objects are generated with Poisson-disk sampling using a dart-throwing approach based on [CJW*09]. Our implementation is fully parallelized [IABT11], and the experiments were run on a 16-core Intel Xeon CPU with 3.10 GHz. The scenes were rendered using Houdini's physically based Mantra renderer [Sid16] at 50 frames per second.
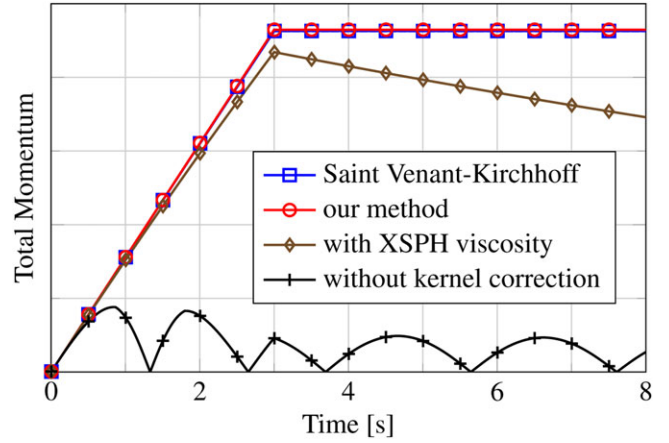

Figure 2: *Momentum of a cube during and after 3 s within a rotational force field. Our rotation handling is of similar accuracy compared to the non-linear Saint Venant–Kirchhoff model. Employing XSPH viscosity damps rotation. Not employing the kernel correction suppresses rotation.*
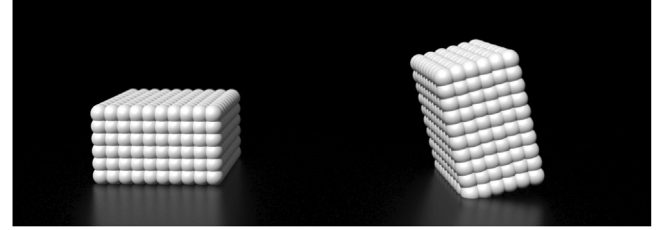

Figure 3: *Two cuboids falling onto a plane. For the cuboid on the right, kernel correction is disabled, which prevents it from rotating.*

5.1. Rotation handling

We compare the rotation handling of our implicit formulation to a Saint Venant-Kirchhoff model which uses the non-linear, rotation invariant Green strain tensor. We further compare to our formulation without kernel correction and to our formulation with an additional small XSPH viscosity force. In the experiment, a deformable cube is accelerated for 3 s in a rotational force field. The plot in Figure 2 shows the resulting total momentum. Our method shows the same perfect rotation conservation as the Saint Venant-Kirchhoff model. However, when further employing an XSPH viscosity force, as it is typically done in practice, rotation is damped. Without kernel correction, the cube is pulled back to its original orientation and rotation is suppressed.

This is further illustrated with the scene in Figure 3, where two initially slightly rotated cuboids fall onto a plane. Whereas the cuboid with kernel correction is able to rotate freely and to adjust its orientation to match the plane orientation, the cuboid without kernel correction is pulled back to its initial orientation and is hindered from adjusting to the plane orientation.
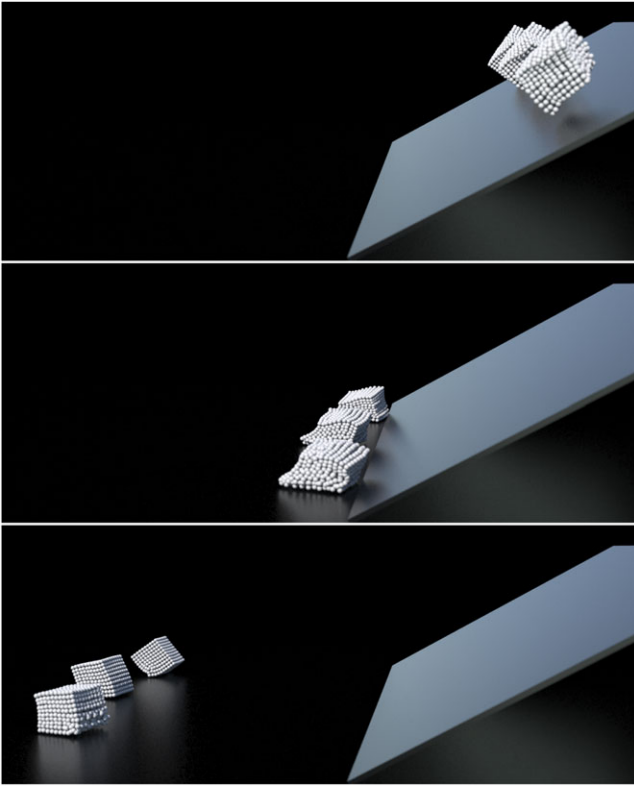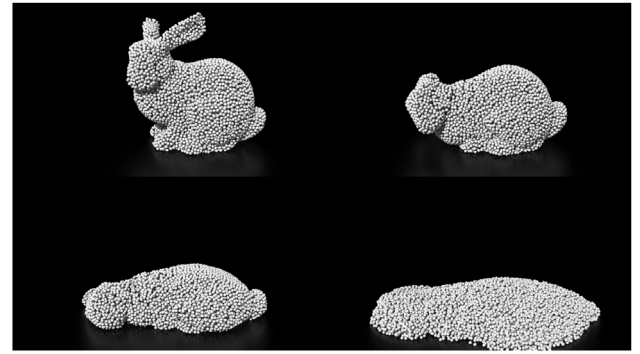
Figure 4: *Comparison to Saint Venant–Kirchhoff. The nearest cuboid is simulated with the Saint Venant–Kirchhoff model. The cuboid in the middle is simulated with our method using the same timestep. The farthest cuboid is simulated with our method using a timestep that is five times larger.*

(a) Our implicit formulation

(b) Becker et al.

Figure 5: *Comparison of our implicit formulation to the method of Becker et al. [BIT09]. The overall simulation behaviour is comparable. The method of Becker et al. is unstable for high shear and bulk moduli. In this scenario, the performance gain factor of our method compared to Becker et al. is more than one hundred.*

5.2. Comparison to Saint Venant–Kirchhoff

In the scene shown in Figure 4, we compare our method to the non-linear Saint VenantKirchhoff model in a more complex scenario. When both simulations run with the same timestep, our method shows comparable behaviour. We also note that our method shows smaller local oscillations compared to Saint Venant–Kirchhoff. When the timestep of our method is increased, the behaviour slightly diverges. This is not only due to our linear approximation in time, but also due to the pressure solver and the viscous force, whose behaviour is timestep dependent.

5.3. Comparison to Becker *et al.* [BIT09]

The experiment shown in Figure 5 consists of a bunny whose shear and bulk modulus are first decreased gradually and then increased again. We did the same experiment replacing our implicit formulation by the method of Becker *et al.* [BIT09]. The overall behaviour of the bunny is comparable for both methods. Nevertheless, although a timestep smaller by a factor of two hundred was chosen, the simulation using the method of Becker *et al.* is unstable for high shear and bulk moduli. These instabilities could only be removed by increasing viscosity or by reducing the timestep further. Therefore, with the method of Becker *et al.* we were not able to get a stable

simulation while preserving small-scale details. Furthermore, with the given parameters, the method of Becker *et al.* was 108 times slower compared to our implicit formulation.

5.4. Parameter evaluation

The scenario in Figure 6 illustrates the influence of shear and bulk modulus. It consists of three parts, and in each part three armadillos with different parameters fall onto a plane. In the first experiment, the shear modulus is equal for all armadillos, while the bulk modulus varies. In the second experiment, the bulk modulus is equal and the shear modulus varies. In the third experiment, shear and bulk modulus are set to the same magnitude for each armadillo, but vary amongst the armadillos. Table 1 summarizes the set-up and the results. The images and timings indicate that matching the bulk modulus to the shear modulus gives convincing results at a fair cost. Therefore, in the following experiments, we will typically set both moduli to match.

5.5. Phase transition

Figure 7 shows a scenario where a bunny dissolves into liquid with shear and bulk modulus set to zero. After that, it is reassembled

Table 1: *Scene parameters and performance data of the simulated scenarios. Two readings in the 'particles' column indicate the number of deformable and water particles, respectively. Square brackets in the 'G' and 'K' column indicate matching shear and bulk moduli. The timings given in the last column represent the total time for computing one frame, that is, the time needed to advance the simulation by 20 ms.*

Scene		Figure	Particles	Spacing (m)	G (Pa)	K (Pa)	Δt (ms)	Average iterations def.	press.	time/frame (s)
Comparison	StVK				$[1 \times 10^4]$		1.0	–	1	0.033
	Our method	Figure 4	1k	0.05	$[1 \times 10^4]$		1.0	1	1	0.041
	Our method						5.0	3	3.6	0.014
Comparison	Becker *et al.*	Figure 5	15k	0.04	$[5 \times 10^2 - 5 \times 10^5]$		0.01	–	1	40.1
	Our method						2.0	18	1.4	0.37
Parameter evaluation		Figure 6	129k	0.05	2×10^3 2×10^5 2×10^7	2×10^5	1.0	3 7 80	1	8.3
					2×10^3 2×10^5 2×10^7	2×10^5	1.0	5 7 59	1	6.4
					2×10^3 2×10^5 2×10^7	2×10^3 2×10^5 2×10^7	1.0	1 7 89	1	8.4
Phase trans.	Bunny	Figure 7	15k	0.04	$[0 - 5 \times 10^4]$		2.0	6	1.2	0.22
	Armadillos	Figure 8	123k	0.03	$[0 - 2 \times 10^5]$		1.4	10	17	4.3
Self-collision		Figure 9	58k	0.0125	5×10^2	5×10^3	1.0	3	1	0.87
Coupling	$2 \times 10^2 \mathrm{kg\,m^{-3}}$							13.6	1.0	0.57
	$2 \times 10^3 \mathrm{kg\,m^{-3}}$	Figure 10	11k	0.05	2×10^5	2×10^6	1.0	13.5	1.0	0.58
	$2 \times 10^4 \mathrm{kg\,m^{-3}}$							14.1	1.1	0.61
Multi-phase		Figure 11	135k + 278k	0.05	$[3 \times 10^4 - 1 \times 10^6]$		2.0	34	6	3.9
Large scale		Figure 12	1M + 4.6M	0.025	$[2 \times 10^4]$		1.0	43	8	112

as shear and bulk modulus are increased. Our implicit formulation is able to cope with large particle displacements that result from the dissolution. This is further illustrated with the scenario in Figure 8, where four armardillos in a box dissolve into fluid and are hereupon reassembled sequentially. Whereas the iteration count in Table 1 reveals that for most other scenarios the pressure solver is not challenged, it needs an increased number of iterations in the present scenario, as it is responsible for separating the armadillos. This is further aggravated by the fact that the armadillos cannot fully unfold to their rest shape due to the limited space available in the closed box.

5.6. Self-collision

With the scenario in Figure 9, the capability of detecting and re-solving self-collisions is illustrated with a cloth-like object falling onto a solid sphere. The object consists of one layer of particles only. To get a stable simulation, an additional zero-energy mode suppression force [Gan15] is applied. As for cloth-like materials, bending is desired whereas stretching is not, the bulk modulus is set to a higher value than the shear modulus in this scene as stated in Table 1.

5.7. Two-way coupling

The scenario in Figure 10 illustrates two-way coupling of our deformables formulation with solid objects of different densities. A deformable bunny with a density of 1000 kg m^{-3} is hit by a fast-moving capsule-shaped object. The scenario is simulated three times with the density of the capsule set to 200 kg m^{-3}, 2000 kg m^{-3} and 20 000 kg m^{-3}, respectively. As shown in Table 1, the performance is comparable for all three simulations. Interestingly, in contrast to multi-phase simulations, the pressure solver is not challenged in this scenario. This is probably due to the short time span the capsule and the bunny are in direct contact. To prevent the capsule from penetrating the bunny, the bulk modulus is increased compared to the shear modulus in this scenario.

5.8. Multi-phase

Figure 11 shows a scenario where deformable objects with different shear and bulk moduli interact. Furthermore, they interact with a water-like phase, where both shear and bulk modulus are set to zero. The water phase has a density of 1000 kg m^{-3}. The white-coloured phase has the moduli set to $G = K = 3 \times 10^4$ Pa and a density of 333 kg m^{-3}, whereas for
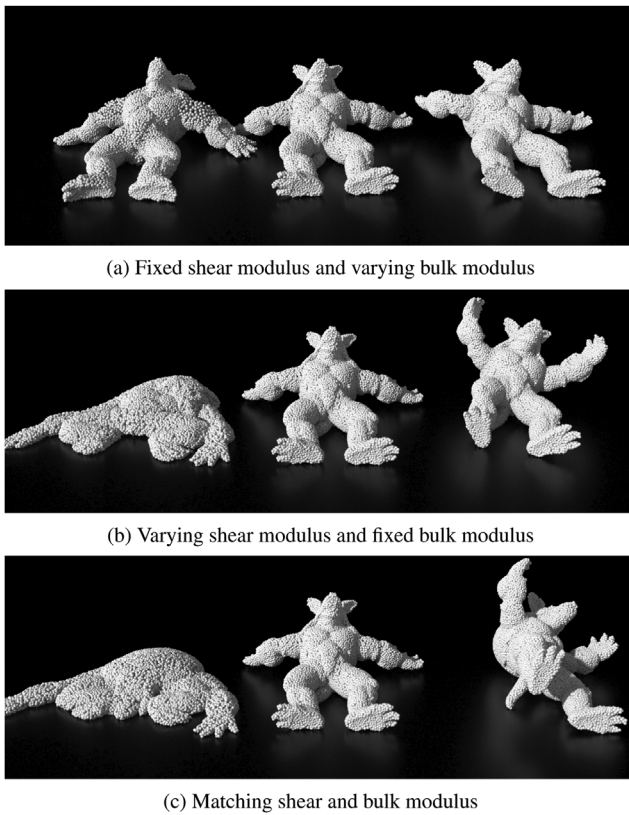
(a) Fixed shear modulus and varying bulk modulus

(b) Varying shear modulus and fixed bulk modulus

(c) Matching shear and bulk modulus

Figure 6: *Illustration of the influence of bulk and shear modulus.*
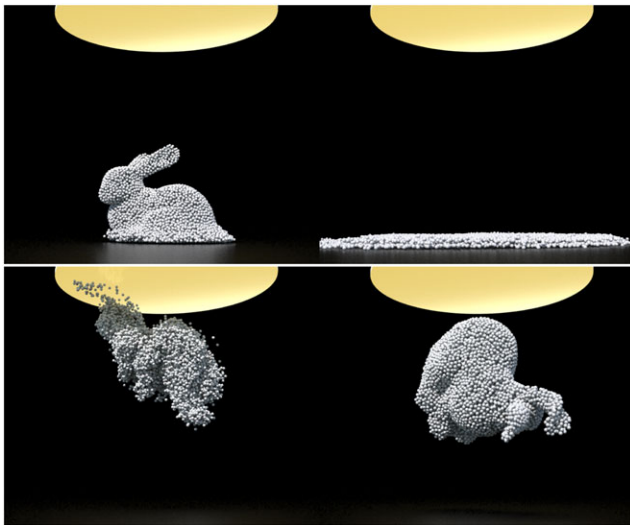
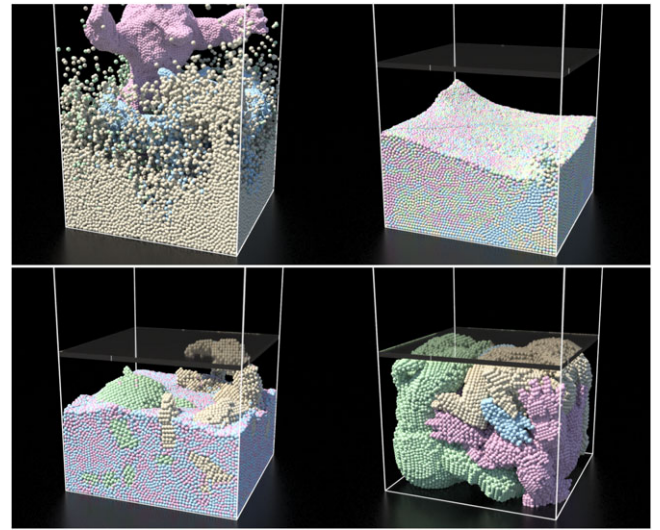**Figure 7:** *A bunny dissolves into a liquid and is reassembled thereafter.*

Figure 8: *Four armadillos in a box dissolve into liquid and are then reassembled sequentially.*
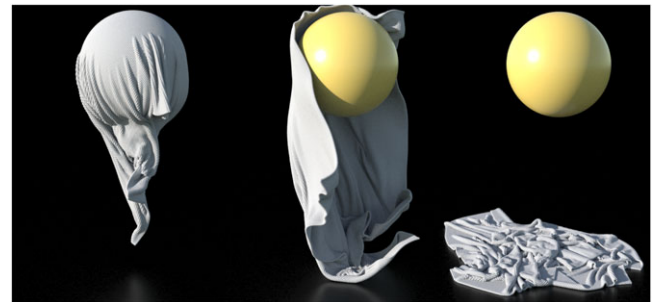

Figure 9: *A piece of cloth slides over a sphere and falls to the ground. This employs various self-collision, which are handled by the pressure solver.*
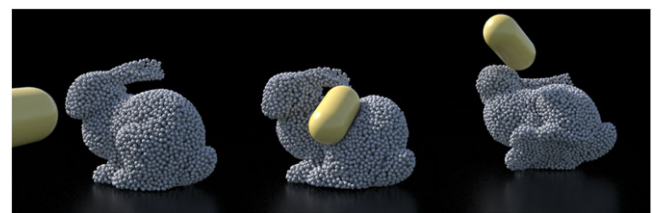

Figure 10: *A deformable bunny is shot by a rigid capsule. The interaction is accomplished by the pressure solver.*

the pressure solver is more challenged, as it has to separate the phases.

5.9. Large scale

The scenario in Figure 12 consists of a deformable hairball [McG11] with a density of 300 kg m^{-3} that is sampled with 1M
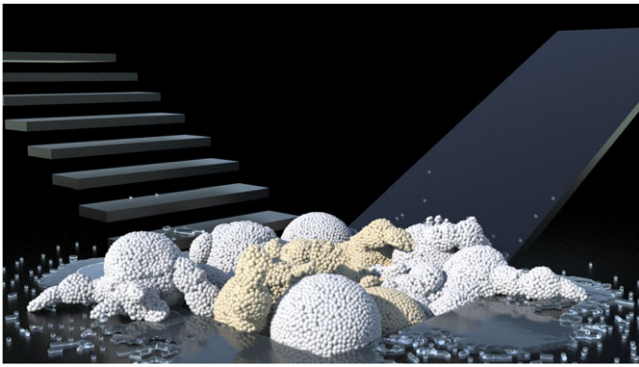
the yellow-coloured phase, $G = K = 1 \times 10^6$ Pa, and the density is 666 kg m^{-3}. Apart from showing the interaction between the phases, the scenario also illustrates the rotation handling of our approach. In contrast to the previous scenarios with one phase,

Although we have achieved an efficiency gain factor of up to one hundred compared to [BIT09], there are still limiting factors for the timestep that could be addressed. In particular, our implementation employs rather large explicit friction forces at the rigid interface that limit the overall performance. Another limiting factor is the maximum density ratio between different phases. Here, we only work with small ratios of one order of magnitude not to negatively affect the performance.

Figure 11: *Multiple deformable armadillos, bunnies and spheres slide, roll and fall into a pool of water. The interaction between the different objects, as well as the interaction with the water, is accomplished by the pressure solver.*
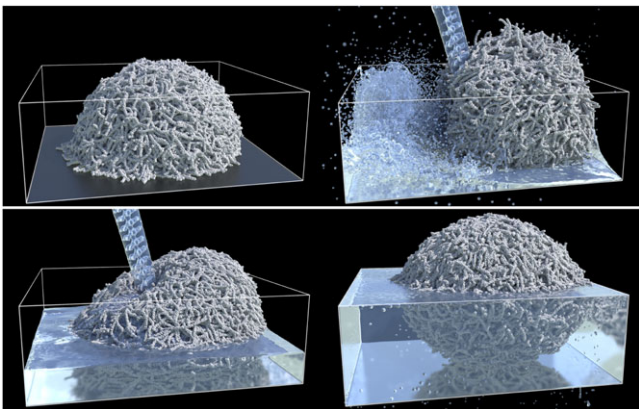

Figure 12: *A deformable hairball is flooded with water. The hairball is sampled from a complex geometry that includes channels and cavities. The scenarios consists of up to 5.6M particles.*

particles. It interacts with up to 4.6M fluid particles with a density of 1000 kg m^{-3}. As revealed by Table 1, simulating one frame of this scenario took less than 2 min. Furthermore, the scenario shows the ability to efficiently represent deformable objects with complex geometry.

6. Conclusion

We have presented a novel SPH formulation for elastic solids. In contrast to previous work, kernel-gradient correction is employed to enable the rotation extraction from an SPH deformation gradient. Comparisons with the nonlinear Saint Venant–Kirchhoff model indicate the accuracy of the proposed rotation handling. We have further introduced an implicit formulation for the velocity update that significantly improves the performance compared to [BIT09], a previous SPH formulation for elastic solids. The embedding of our approach into an ISPH fluid solver [ICS*14] elegantly accounts for boundary handling, self-collisions, phase transitions and multi-phase fluids.

References

[AAT13] AKINCI N., AKINCI G., TESCHNER M.: Versatile surface tension and adhesion for SPH fluids. *ACM Transactions on Graphics (TOG) 32*, 6 (2013), 182:1–182:8.

[AIA*12] AKINCI N., IHMSEN M., AKINCI G., SOLENTHALER B., TESCHNER M.: Versatile rigid-fluid coupling for incompressible SPH. *ACM Transactions on Graphics (TOG) 31*, 4 (2012), 62:1–62:8.

[BFA02] BRIDSON R., FEDKIW R., ANDERSON J.: Robust treatment of collisions, contact and friction for cloth animation. *ACM Transactions on Graphics (TOG) 21*, 3 (2002), 594–603.

[BGLX00] BELYTSCHKO T., GUO Y., LIU W. K., XIAO S. P.: A unified stability analysis of meshless particle methods. *International Journal for Numerical Methods in Engineering 48*, 9 (2000), 1359–1400.

[BIT09] BECKER M., IHMSEN M., TESCHNER M.: Corotated SPH for deformable solids. In *Eurographics Workshop on Natural Phenomena*. E. Galin and J. Schneider (Eds.). The Eurographics Association, Aire-la-Ville, Switzerland (2009), pp. 27–34.

[BK01] BONET J., KULASEGARAM S.: Remarks on tension instability of Eulerian and Lagrangian corrected smooth particle hydrodynamics (CSPH) methods. *International Journal for Numerical Methods in Engineering 52*, 11 (2001), 1203–1220.

[BK16] BENDER J., KOSCHIER D.: Divergence-free SPH for incompressible and viscous fluids. *IEEE Transactions on Visualization and Computer Graphics 23*, 3 (2016), 1193–1206.

[BKCW14] BENDER J., KOSCHIER D., CHARRIER P., WEBER D.: Position-based simulation of continuous materials. *Computers & Graphics 44* (2014), 1–10.

[BL99] BONET J., LOK T.-S.: Variational and momentum preservation aspects of smooth particle hydrodynamic formulations. *Computer Methods in Applied Mechanics and Engineering 180*, 1 (1999), 97–115.

[BML*14] BOUAZIZ S., MARTIN S., LIU T., KAVAN L., PAULY M.: Projective dynamics: Fusing constraint projections for fast simulation. *ACM Transactions on Graphics (TOG) 33*, 4 (2014), 154:1–154:11.

[BMO*14] BENDER J., MÜLLER M., OTADUY M. A., TESCHNER M., MACKLIN M.: A survey on position-based simulation methods in

computer graphics. In *Computer Graphics Forum 33*, 6 (2014), 228–251.

[BW98] BARAFF D., WITKIN A.: Large steps in cloth simulation. In *Proceedings of the 25th Annual Conference on Computer Graphics and Interactive Techniques* (New York, NY, USA, 1998), ACM, pp. 43–54.

[CBP05] CLAVET S., BEAUDOIN P., POULIN P.: Particle-based viscoelastic fluid simulation. In *Proceedings of the 2005 ACM SIGGRAPH/Eurographics Symposium on Computer Animation* (New York, NY, USA, 2005), ACM, pp. 219–228.

[CJW*09] CLINE D., JESCHKE S., WHITE K., RAZDAN A., WONKA P.: Dart throwing on surfaces. *Computer Graphics Forum, 28* (2009), 1217–1226.

[CMM16] CHENTANEZ N., MÜLLER M., MACKLIN M.: Real-time simulation of large elasto-plastic deformation with shape matching. In *Proceedings of the ACM SIGGRAPH/Eurographics Symposium on Computer Animation* (Aire-la-Ville, Switzerland, 2016), Eurographics Association, pp. 159–167.

[CPDH12] CLEARY P. W., PRAKASH M., DAS R., HA J.: Modelling of metal forging using SPH. *Applied Mathematical Modelling 36*, 8 (2012), 3836–3855.

[DA12] DEHNEN W., ALY H.: Improving convergence in smoothed particle hydrodynamics simulations without pairing instability. *Monthly Notices of the Royal Astronomical Society 425*, 2 (2012), 1068–1082.

[DG96] DESBRUN M., GASCUEL M.-P.: Smoothed particles: A new paradigm for animating highly deformable bodies. *Computer Animation and Simulation 96* (1996), 61–76.

[DGP12] DAGENAIS F., GAGNON J., PAQUETTE E.: A prediction-correction approach for stable SPH fluid simulation from liquid to rigid. In *Proceedings of the Computer Graphics International 2012* (Bournemouth, England, UK, 2012).

[DGW11] DICK C., GEORGII J., WESTERMANN R.: A hexahedral multigrid approach for simulating cuts in deformable objects. *IEEE Transactions on Visualization and Computer Graphics 17*, 11 (2011), 1663–1675.

[Gan15] GANZENMÜLLER G. C.: An hourglass control algorithm for Lagrangian smooth particle hydrodynamics. *Computer Methods in Applied Mechanics and Engineering 286* (2015), 87–106.

[GBB09] GERSZEWSKI D., BHATTACHARYA H., BARGTEIL A. W.: A point-based method for animating elastoplastic solids. In *Proceedings of the 2009 ACM SIGGRAPH/Eurographics Symposium on Computer Animation* (New York, NY, USA, 2009), ACM, pp. 133–138.

[GBP*17] GISSLER C., BAND S., PEER A., IHMSEN M., TESCHNER M.: Generalized drag force for particle-based simulations. *Computers & Graphics 69* (2017), 1–11.

[GHM15] GANZENMÜLLER G. C., HIERMAIER S., MAY M.: On the similarity of meshless discretizations of peridynamics and smooth-particle hydrodynamics. *Computers & Structures 150* (2015), 71–78.

[GSMH16] GANZENMÜLLER G. C., SAUER M., MAY M., HIERMAIER S.: Hourglass control for smooth particle hydrodynamics removes tensile and rank-deficiency instabilities. *The European Physical Journal Special Topics 225*, 2 (2016), 385–395.

[HWW17] HE X., WANG H., WU E.: Projective peridynamics for modeling versatile elastoplastic materials. *IEEE Transactions on Visualization and Computer Graphics* (2017). https://doi.org/10.1109/TVCG.2017.2755646.

[IABT11] IHMSEN M., AKINCI N., BECKER M., TESCHNER M.: A parallel SPH implementation on multi-core CPUs. *Computer Graphics Forum 30* (2011), 99–112.

[ICS*14] IHMSEN M., CORNELIS J., SOLENTHALER B., HORVATH C., TESCHNER M.: Implicit incompressible SPH. *IEEE Transactions on Visualization and Computer Graphics 20*, 3 (2014), 426–435.

[IOS*14] IHMSEN M., ORTHMANN J., SOLENTHALER B., KOLB A., TESCHNER M.: SPH fluids in computer graphics. In *Eurographics 2014-State of the Art Reports* (Strasbourg, France, 2014), The Eurographics Association, pp. 21–42.

[JGT17] JIANG C., GAST T., TERAN J.: Anisotropic elastoplasticity for cloth, knit and hair frictional contact. *ACM Transactions on Graphics (TOG) 36*, 4 (2017), 152:1–152:14.

[JK09] JEŘÁBKOVÁ L., KUHLEN T.: Stable cutting of deformable objects in virtual environments using XFEM. *IEEE Computer Graphics and Applications 29*, 2 (2009), 61–71.

[JWJ*14] JONES B., WARD S., JALLEPALLI A., PERENIA J., BARGTEIL A. W.: Deformation embedding for point-based elastoplastic simulation. *ACM Transactions on Graphics (TOG) 33*, 2 (2014), 21:1–21:9.

[KAG*05] KEISER R., ADAMS B., GASSER D., BAZZI P., DUTRÉ P., GROSS M.: A unified Lagrangian approach to solid-fluid animation. In *Point-Based Graphics, 2005. Eurographics/IEEE VGTC Symposium Proceedings* (Aire-la-Ville, Switzerland, 2005), IEEE, pp. 125–148.

[KBT17] KOSCHIER D., BENDER J., THUEREY N.: Robust eXtended Finite Elements for complex cutting of deformables. *ACM Transactions on Graphics (ACM SIGGRAPH 2017) 36*, 4 (2017), 1–13.

[KMBG09] KAUFMANN P., MARTIN S., BOTSCH M., GROSS M.: Flexible simulation of deformable models using discontinuous Galerkin FEM. *Graphical Models 71*, 4 (2009), 153–167.

[LBK16] LIU T., BOUAZIZ S., KAVAN L.: Towards real-time simulation of hyperelastic materials. arXiv preprint arXiv:1604.07378 (2016).

[LBOK13] LIU T., BARGTEIL A. W., O'BRIEN J. F., KAVAN L.: Fast simulation of mass-spring systems. *ACM Transactions on Graphics (TOG) 32*, 6 (2013), 214:1–214:7.

[LD08] LENAERTS T., DUTRÉ P.: *Unified SPH model for fluid-shell simulations*. Report CW 530, Departement of Computer Science, KU Leuven, Celestijnenlaan 200A, 3001 Heverlee, Belgium, November 2008.

[LD09] LENAERTS T., DUTRÉ P.: *An architecture for unified SPH simulations*. Report CW 559, Departement Computerwetenschappen, KU Leuven, Celestijnenlaan 200A, 3001 Heverlee, Belgium, 2009. [URL: http://www.cs.kuleuven.be/publicaties/rapporten/cw/CW559.abs.html.]

[LS81] LANCASTER P., SALKAUSKAS K.: Surfaces generated by moving least squares methods. *Mathematics of Computation 37*, 155 (1981), 141–158.

[MBCM16] MÜLLER M., BENDER J., CHENTANEZ N., MACKLIN M.: A robust method to extract the rotational part of deformations. In *Proceedings of the 9th International Conference on Motion in Games* (Burlingame, California, 2016), MIG '16, ACM, pp. 55–60.

[MC11] MÜLLER M., CHENTANEZ N.: Solid simulation with oriented particles. *ACM Transactions on Graphics (TOG) 30* (2011), p. 92.

[McG11] MCGUIRE M.: Computer graphics archive, August 2011. URL: http://graphics.cs.williams.edu/data.

[MDM*02] MÜLLER M., DORSEY J., MCMILLAN L., JAGNOW R., CUTLER B.: Stable real-time deformations. In *Proceedings of the 2002 ACM SIGGRAPH/Eurographics Symposium on Computer Animation* (2002), ACM, pp. 49–54.

[MFZ97] MORRIS J. P., FOX P. J., ZHU Y.: Modeling low Reynolds number incompressible flows using SPH. *Journal of Computational Physics 136*, 1 (1997), 214–226.

[MHHR07] MÜLLER M., HEIDELBERGER B., HENNIX M., RATCLIFF J.: Position based dynamics. *Journal of Visual Communication and Image Representation 18*, 2 (2007), 109–118.

[MHTG05] MÜLLER M., HEIDELBERGER B., TESCHNER M., GROSS M.: Meshless deformations based on shape matching. *ACM Transactions on Graphics (TOG) 24*, 3 (2005), 471–478.

[MKB*10] MARTIN S., KAUFMANN P., BOTSCH M., GRINSPUN E., GROSS M.: Unified simulation of elastic rods, shells, and solids. *ACM Transactions on Graphics (TOG) 29*, 4 (2010), 39.

[MKN*04] MÜLLER M., KEISER R., NEALEN A., PAULY M., GROSS M., ALEXA M.: Point based animation of elastic, plastic and melting objects. In *Proceedings of the 2004 ACM SIGGRAPH/Eurographics Symposium on Computer Animation* (2004), Eurographics Association, pp. 141–151.

[MM13] MACKLIN M., MÜLLER M.: Position based fluids. *ACM Transactions on Graphics (TOG) 32*, 4 (2013), 104.

[MMC16] MACKLIN M., MÜLLER M., CHENTANEZ N.: XPBD: position-based simulation of compliant constrained dynamics. In *Proceedings of the 9th International Conference on Motion in Games* (2016), ACM, pp. 49–54.

[MMCK14] MACKLIN M., MÜLLER M., CHENTANEZ N., KIM T.-Y.: Unified particle physics for real-time applications. *ACM Transactions on Graphics (TOG) 33*, 4 (2014), 153.

[Mon89] MONAGHAN J.: On the problem of penetration in particle methods. *Journal of Computational Physics 82*, 1 (1989), 1–15.

[Mon92] MONAGHAN J. J.: Smoothed particle hydrodynamics. *Annual Review of Astronomy and Astrophysics 30* (1992), 543–574.

[Mon12] MONAGHAN J.: Smoothed particle hydrodynamics and its diverse applications. *Annual Review of Fluid Mechanics 44* (2012), 323–346.

[MP89] MILLER G., PEARCE A.: Globular dynamics: A connected particle system for animating viscous fluids. *Computers & Graphics 13*, 3 (1989), 305–309.

[NMK*06] NEALEN A., MÜLLER M., KEISER R., BOXERMAN E., CARLSON M.: Physically based deformable models in computer graphics. *Computer Graphics Forum 25* (2006), 809–836.

[NOB16] NARAIN R., OVERBY M., BROWN G. E.: ADMM ⊇ projective dynamics: Fast simulation of general constitutive models. In *Proceedings of the ACM SIGGRAPH/Eurographics Symposium on Computer Animation* (2016), Eurographics Association, pp. 21–28.

[PICT15] PEER A., IHMSEN M., CORNELIS J., TESCHNER M.: An implicit viscosity formulation for SPH fluids. *ACM Transactions on Graphics (TOG) 34*, 4 (2015), 114.

[PKA*05] PAULY M., KEISER R., ADAMS B., DUTRÉ P., GROSS M., GUIBAS L. J.: Meshless animation of fracturing solids. *ACM Transactions on Graphics (TOG) 24*, 3 (2005), 957–964.

[PT17] PEER A., TESCHNER M.: Prescribed velocity gradients for highly viscous SPH fluids with vorticity diffusion. *IEEE Transactions on Visualization and Computer Graphics 23*, 12 (Dec2017), 2656–2662.

[RLY*14] REN B., LI C., YAN X., LIN M. C., BONET J., HU S.-M.: Multiple-fluid SPH simulation using a mixture model. *ACM Transactions on Graphics (TOG) 33*, 5 (2014), 171.

[SB12a] SCHECHTER H., BRIDSON R.: Ghost SPH for animating water. *ACM Transactions on Graphics (TOG) 31*, 4 (2012), 61.

[SB12b] SIFAKIS E., BARBIC J.: FEM simulation of 3D deformable solids: a practitioner's guide to theory, discretization and model reduction. In *ACM SIGGRAPH 2012 Courses* (2012), ACM, p. 20.

[Sid16] SIDE EFFECTS SOFTWARE: Houdini, 2016. URL: http://www.sidefx.com.

[Sil00] SILLING S. A.: Reformulation of elasticity theory for discontinuities and long-range forces. *Journal of the Mechanics and Physics of Solids 48*, 1 (2000), 175–209.

[SP08] SOLENTHALER B., PAJAROLA R.: Density contrast SPH interfaces. In *Proceedings of the 2008 ACM SIGGRAPH/Eurographics Symposium on Computer Animation* (2008), Eurographics Association, pp. 211–218.

[SSF13] SU J., SHETH R., FEDKIW R.: Energy conservation for the simulation of deformable bodies. *IEEE Transactions on Visualization and Computer Graphics 19*, 2 (2013), 189–200.

[SSJ*14] STOMAKHIN A., SCHROEDER C., JIANG C., CHAI L., TERAN J., SELLE A.: Augmented MPM for phase-change and varied materials. *ACM Transactions on Graphics (TOG) 33*, 4 (2014), 138.

[SSP07] SOLENTHALER B., SCHLÄFLI J., PAJAROLA R.: A unified particle model for fluid–solid interactions. *Computer Animation and Virtual Worlds 18*, 1 (2007), 69–82.

[TDF*15] TAKAHASHI T., DOBASHI Y., FUJISHIRO I., NISHITA T., LIN M. C.: Implicit formulation for SPH-based viscous fluids. *Computer Graphics Forum 34* (2015), 493–502.

[TDFN16] TAKAHASHI T., DOBASHI Y., FUJISHIRO I., NISHITA T.: Volume preserving viscoelastic fluids with large deformations using position-based velocity corrections. *The Visual Computer 32*, 1 (2016), 57–66.

[THMG04] TESCHNER M., HEIDELBERGER B., MULLER M., GROSS M.: A versatile and robust model for geometrically complex deformable solids. In *Computer Graphics International, 2004. Proceedings* (2004), IEEE, pp. 312–319.

[TL16] TAKAHASHI T., LIN M. C.: A multilevel SPH solver with unified solid boundary handling. *Computer Graphics Forum 35* (2016), 517–526.

[TPF89] TERZOPOULOS D., PLATT J., FLEISCHER K.: From goop to glop: Heating and melting deformable models. *Proceedings Graphics Interface 2*, 2 (June1989), 219–226.

[Wen95] WENDLAND H.: Piecewise polynomial, positive definite and compactly supported radial functions of minimal degree. *Advances in Computational Mathematics 4*, 1 (1995), 389–396.

[WHP*06] WICKE M., HATT P., PAULY M., MÜLLER M., GROSS M.: Versatile virtual materials using implicit connectivity. In *Proceedings of the Eurographics Symposium on Point-Based Graphics* (2006), pp. 137–144.

[WKB16] WEILER M., KOSCHIER D., BENDER J.: Projective fluids. In *Proceedings of the 9th International Conference on Motion in Games* (2016), ACM, pp. 79–84.

[ZLKW13] ZHOU Y., LUN Z., KALOGERAKIS E., WANG R.: Implicit integration for particle-based simulation of elasto-plastic solids. *Computer Graphics Forum 32* (2013), 215–223.

Supporting Information

Additional Supporting Information may be found in the online version of this article at the publisher's web site:

Video S1